X-ray micro-tomographic characterization of field-structured magnetorheological elastomers



2012 Smart Mater. Struct. 21 015005

(http://iopscience.iop.org/0964-1726/21/1/015005)

Smart Mater. Struct. **21** (2012) 015005 (7pp) doi:10.1088/0964-1726/21/1/015005

# X-ray micro-tomographic characterization of field-structured magnetorheological elastomers

**D Günther, D Yu Borin, S Günther and S Odenbach**

Technische Universität Dresden, Institute of Fluid Mechanics, 01062, Dresden, Germany

E-mail: dmitry.borin@tu-dresden.de

Received 6 July 2011, in final form 21 October 2011
Published 7 December 2011
Online at stacks.iop.org/SMS/21/015005

**Abstract**
Anisotropic magnetorheological elastomers (MREs) with four different mass percentages of iron powder were prepared in an external magnetic field. The inner structure of the samples was characterized by using computed tomography. It has been shown that this kind of non-destructive analysis of MRE samples can be efficiently used for a detailed structural investigation. It was found that even small changes in the mass content of the magnetic filler led to the formation of completely different morphologies, which were reproducible for all samples. There were the familiar column formations in patterns with a mass content of ∼5% iron powder. Increasing the mass fraction to ∼14% resulted in the formation of tubular structures. Samples with ∼23 and ∼33 wt% had a densely packed structure, where the particle formations broke up: meanders without particles penetrate the samples over the entire height like canyons.

(Some figures may appear in colour only in the online journal)

## 1. Introduction

Magnetorheological elastomers (MREs) are a kind of smart material and they are receiving more and more attention for technical applications [1]. They are multiphase multifunctional composites consisting of an elastic matrix filled with micron-sized magnetic particles [2]. In this study, anisotropic MREs, which are known to exhibit a larger MR-effect [3], were produced and the dependence of their internal structure on mass content of magnetic material has been investigated. For this purpose a magnetic field was applied during the polymerization process. Due to dipole–dipole interaction the magnetically active particles form chain-like structures. Thereby the chain axis is in line with the field direction [4]. It is also possible that chains connect to form various morphologies depending on the magnetic field strength or the particle volume concentration as is known from magnetorheological fluids [5].

Many publications have already dealt with the mechanical properties of this class of materials [6, 7, 9]. However, the characterization of the structural composition of MREs has been considered very poor up to now, although it represents the fundamental basis for the understanding of the observed mechanical behavior. According to [10], sporadic attempts have been made to analyze the inner structure of isotropic and anisotropic MREs using electron microscopic methods. Single investigations were also conducted with scanning electron microscopy (SEM) [11]. Moreover, light microscopic examinations [7, 8] and x-ray diffraction (XRD) measurements [12] of MRE samples with various iron particle concentrations and magnetic field strengths were performed to determine the phase constitution. These techniques have the inherent disadvantage of sample destruction, which does not allow the subsequent evaluation of the mechanical properties of the MREs. Additionally, they do not allow the analysis of three-dimensional structures. The primary goal of the present work is the structural characterization of anisotropic MREs with different mass concentrations using computed tomography (CT). The characterization by CT not only preserves the structure of the sample but also yields a three-dimensional map of the sample geometry. In this paper MRE samples with a different content of soft magnetic microparticles have been produced and investigated regarding the morphological characteristics of their structures by CT.

 

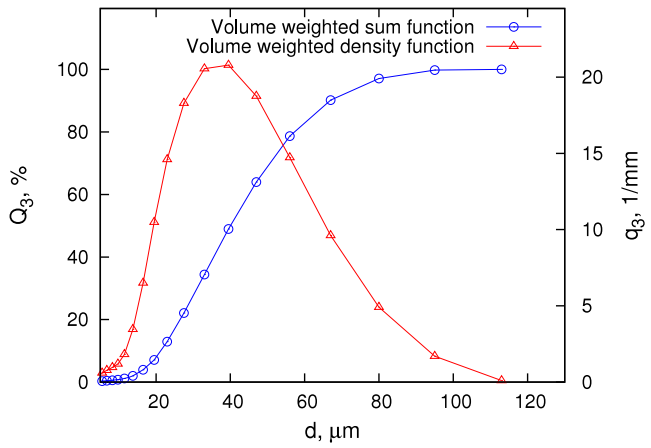


**Figure 1.** Particle size distribution of the used iron powder.

## 2. Materials and sample preparation

### *2.1. Material description*

The polymeric host matrix of the MREs was prepared from the elastomer kit Sylgard 184, provided by the Dow Corning Corporation (USA). Sylgard 184 is a two-component silicone, where the polymerization process is activated by a curing agent. The agent was added in a mass ratio of 1:10. The magnetically soft iron powder ASC200, supplied by Höganäs A B (Sweden), was used as the magnetic active filler of the MREs. For a detailed analysis, the particle size distribution shown in figure 1 was measured by dry dispersion (Rodos system, Sympatec GmbH, Germany) and laser diffraction measurements (Helos system, Sympatec GmbH, Germany). The average particle size is approximately 35 $\mu$m.

### *2.2. Sample preparation*

Anisotropic MREs of four different mass percentages of iron powder were produced (table 1), each with three samples per batch.

**Table 1.** Mass fraction $\phi_m$ of iron powder 'ASC200' inside the samples.

| | |
|---|---|
| $MRE_1$ | 4.6 wt% |
| $MRE_2$ | 13.9 wt% |
| $MRE_3$ | 23.2 wt% |
| $MRE_4$ | 32.8 wt% |

The mixing of the two-component silicone elastomer with the magnetic particles was carried out by mechanical stirring at room temperature until the mixture reached a homogeneous state. Then, the suspension was degassed in a vacuum vessel. Afterward the fluid was transferred to a specially designed sample holder; the magnetic field was applied with an external field strength of 220 kA $m^{-1}$ (Bruker electromagnetic system, Germany). The field was increased by 27.5 kA $m^{-1}$ $s^{-1}$, until the desired field strength was reached. The sample holder was positioned in such a way that all samples were within a region with 99% homogeneity of the magnetic field strength. The field direction was parallel to the longitudinal axis of the cylindrical molds. The required heat quantity for the polymerization process was introduced via a thin current-carrying copper coil on the lateral surface of the sample holder. The generated magnetic field strength of the wire winding was determined to 1900 A $m^{-1}$ and thus was two orders of magnitude less than the applied field and can therefore be neglected in further discussion. The heating process lasted 20 min and was the same for each preparation. The final temperature was 90 $\pm$ 5 °C and was constantly monitored with an infrared thermometer. The entire curing process was completed after 120 min. Figure 2 (left) shows an example of the sample batch $MRE_1$. All samples had a diameter of 30 $\pm$ 1 mm and a height of 15 $\pm$ 1 mm and provided, therefore, a real possibility for the examination of three-dimensional structures inside the MRE.

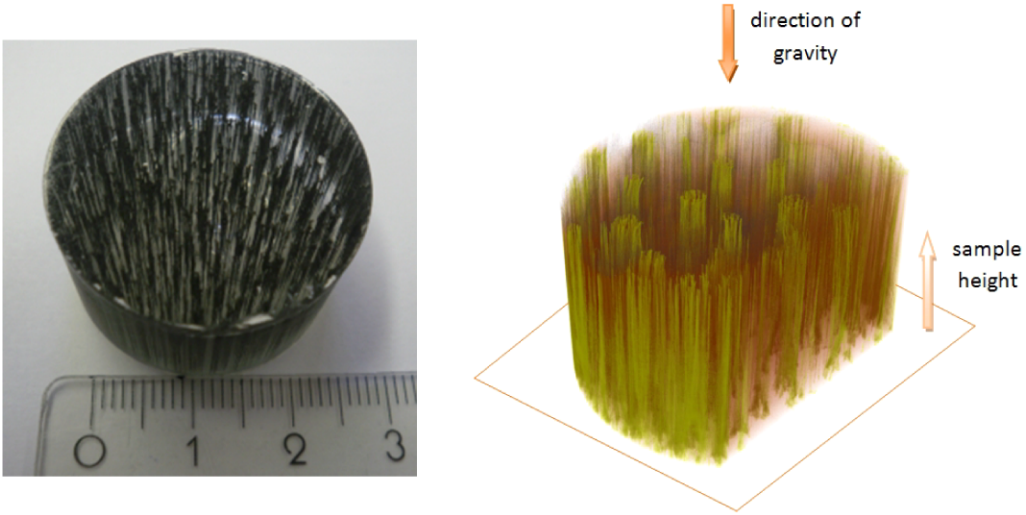


**Figure 2.** Image of sample $MRE_1$ (left) and declaration of the directions for the description in the text for a sample with ~15 wt% (right).

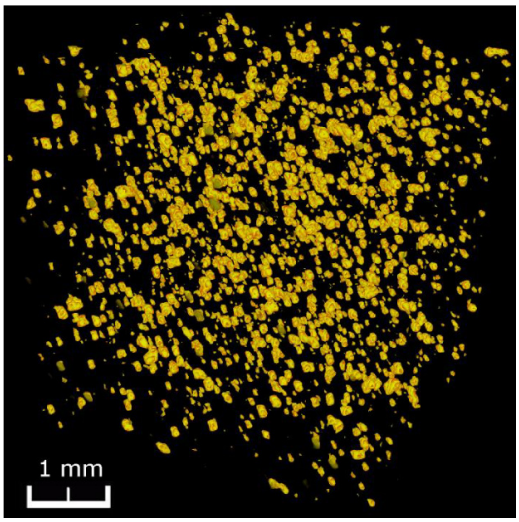


**Figure 3.** Exemplary CT-image of the isotropic MRE sample with ∼5 wt%.

## 3. Characterization with x-ray $\mu$-CT

### *3.1. Examination conditions*

The structure analysis was performed at a CT-imaging system, which is based on a nanofocus tube with the transmission target of the product line phoenix/x-ray (GE Measurement and Control Solutions, USA). The focal spot diameter of the tube is 2 $\mu$m for the used mode. The detection of x-rays is realized by a Shad-o-Box 4K (Rad-icon Imaging Corp., USA), which contains a Gd2O2S scintillator. The photodiode array has 2000 × 2048 (vertical/horizontal) pixels with a pixel spacing of 48 $\mu$m. Projection images were generated with 0.5° angular increment at a tube current of 170–330 $\mu$A and an acceleration voltage of 50–90 kV. The exposure time was varied in accordance with a suitable image quality between 3.5 and 6.8 s for the various tomograms of the sample batches. CT-reconstruction was carried out using VGStudio Max 2.1 by Volume Graphics GmbH (Germany) as evaluation software. For the quantitative analysis the software application ImageJ 1.44n was used.

### *3.2. Structural analysis*

The used x-ray method allows a detailed structural analysis of both isotropic MREs, i.e. prepared without magnetic field, and anisotropic MREs, i.e. field-structured during the cross-linking process. An example of the internal structure of an isotropic sample is shown in figure 3 and the anisotropic sample is depicted in figure 4. Single microparticles and aggregates as well as their spatial position can be identified. As can be seen, the particles are distributed homogeneously in the isotropic sample and form chain-like structures in the anisotropic one.

A detailed structural analysis of the anisotropic samples with different concentration of magnetic powder (table 1) is given below.

Figures 5–8 show cross-sectional CT-images of the samples $MRE_1$, $MRE_2$, $MRE_3$ and $MRE_4$ at three different heights starting from the sample base with respect to the manufacturing process and corresponding 3D-reconstructions of the spatial structure of the particle formations in these samples.

In the $MRE_1$ samples with the lowest mass fraction of iron powder, there is a homogeneous distribution of particle columns. In addition, the formation of isolated column agglomerates could be detected at the middle of the samples. It is remarkable that any variation of the filler concentration results in a completely different morphology. The particle columns of the $MRE_2$ samples self-assemble to tube-like bunches with their longitudinal axis parallel to the magnetic field. In the cross-sectional CT-images these tubes appear as rings that are arranged randomly. However, the distances between them seem to relate to one another at defined intervals.

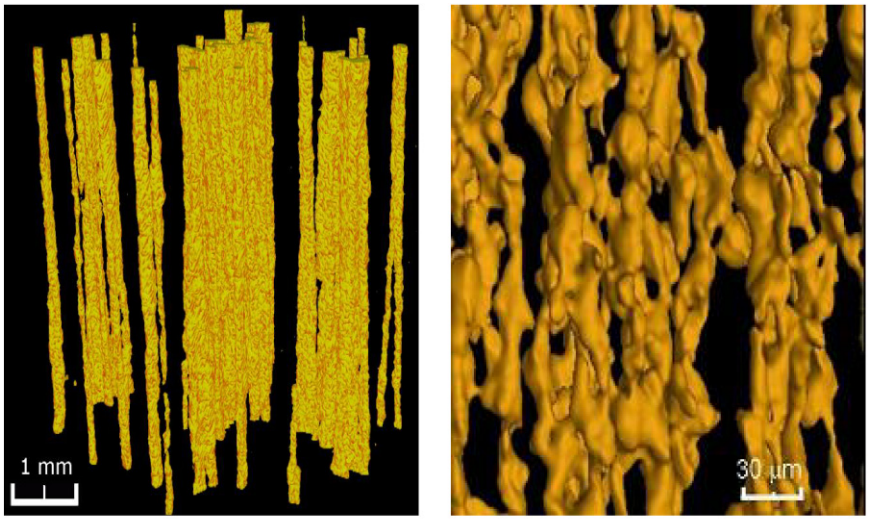


**Figure 4.** Exemplary CT-images of the anisotropic (structured) MRE sample with ∼5 wt% (a) and details of its microstructure (b).

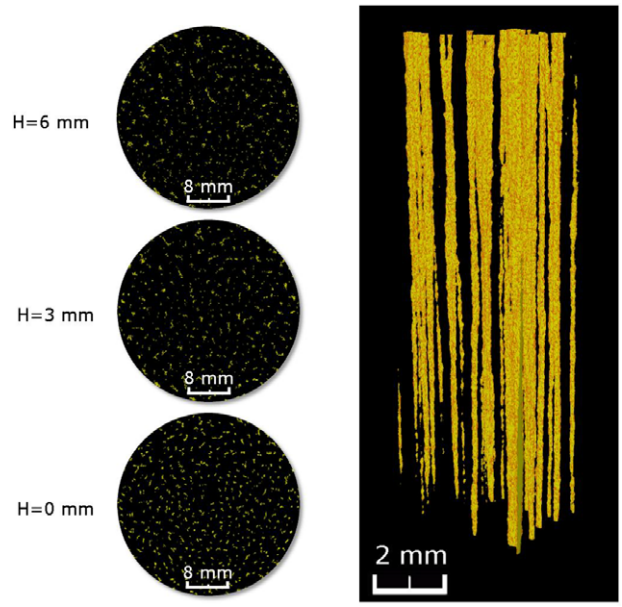


**Figure 5.** Cross-sectional images of the sample $MRE_1$ at three different sample heights (left) and 3D-reconstruction of its columnar structure (right).

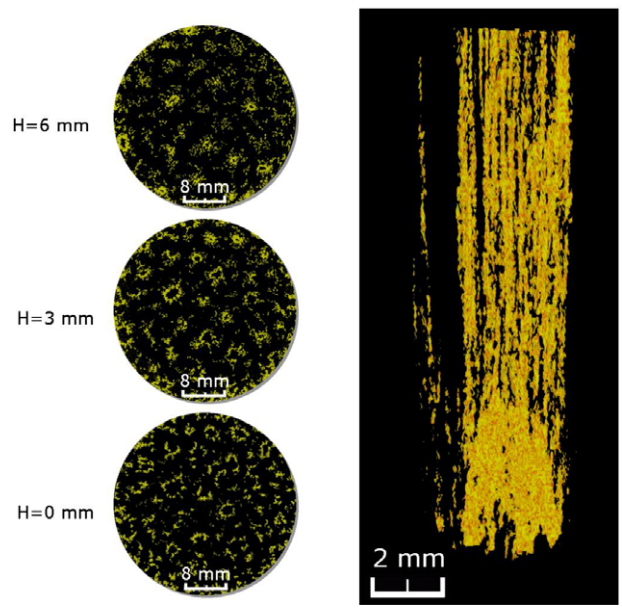


**Figure 6.** Cross-sectional images of the sample $MRE_2$ at three different sample heights (left) and a detailed CT-image of the tube-like formation (right).

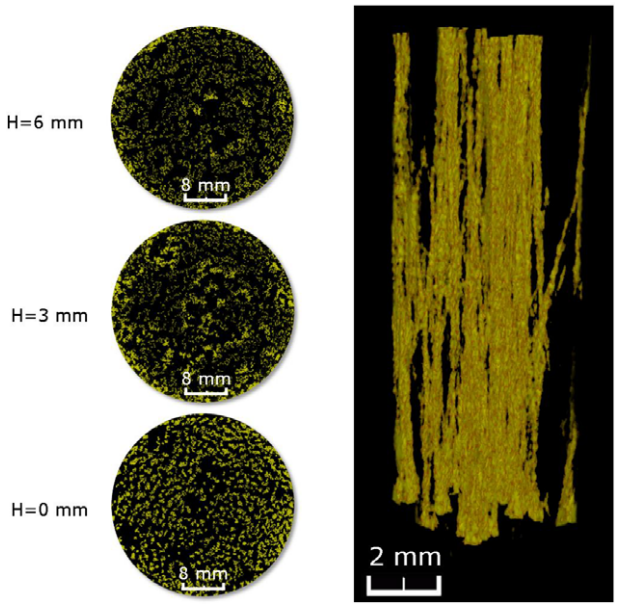


**Figure 7.** Cross-sectional images of the sample $MRE_3$ at three different sample heights (left) and its densely packed structure (right).

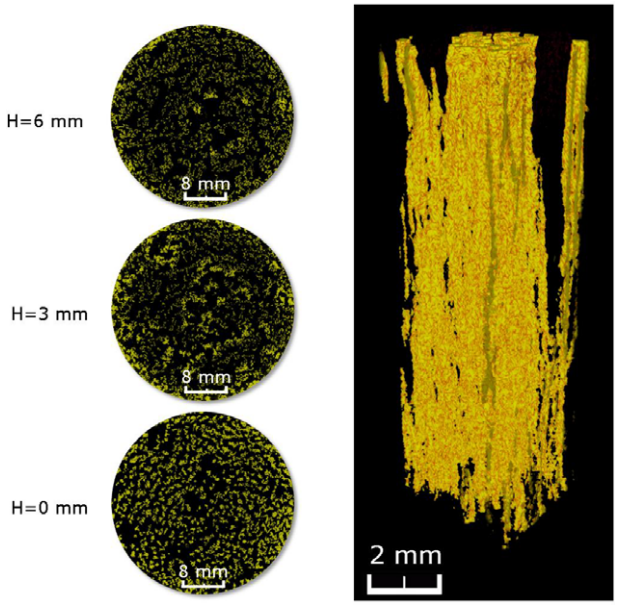


**Figure 8.** Cross-sectional images of the sample $MRE_4$ at three different sample heights (left) and its densely packed structure (right).

At a sample height of 0 mm the tubes have a larger diameter than toward the center of the patterns, where they are almost closed—similar to sheaves that are held together in the middle. The average distance between the tubes of the samples $MRE_2$ is larger than the average distance between the agglomerates in samples $MRE_1$. At a height greater than 6 mm in samples $MRE_2$ column structures are formed again, although the distance between them is significantly lower than those of $MRE_1$ and they are clustered at positions close to the tubes formed at lower heights.

In the samples of the batches $MRE_3$ and $MRE_4$ densely packed structures were formed. There are very thin columns which merge into space branched formations. Also meandering structures arose that penetrated the $MRE_4$ samples over the entire height like canyons. At the inner particle arrangement of the $MRE_3$ samples the first vacancies were found. The inner structure was reproducible for all produced samples.

For a more detailed analysis of the microscopic structure and the arrangement of the particles inside the columns at

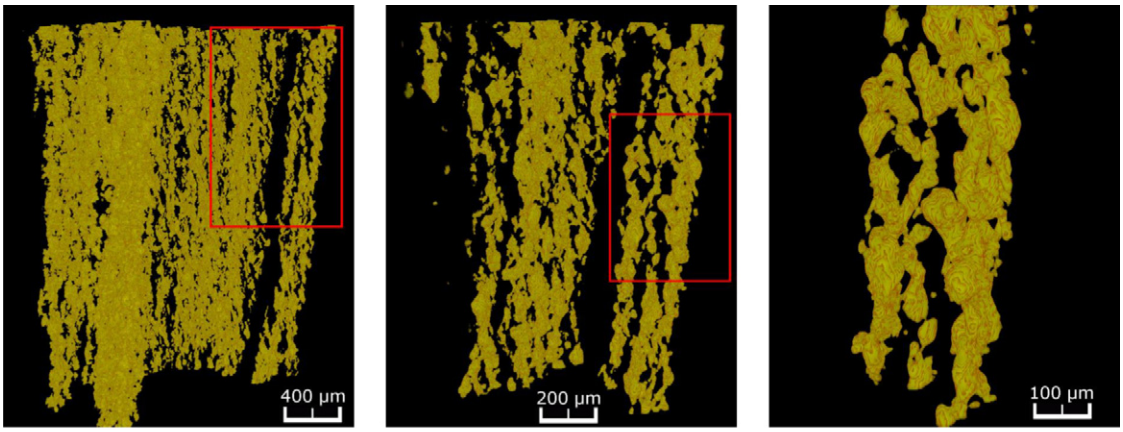


**Figure 9.** Detailed CT-images of the column structure at the top of the rods of figure 6. The red box refers to the next picture.

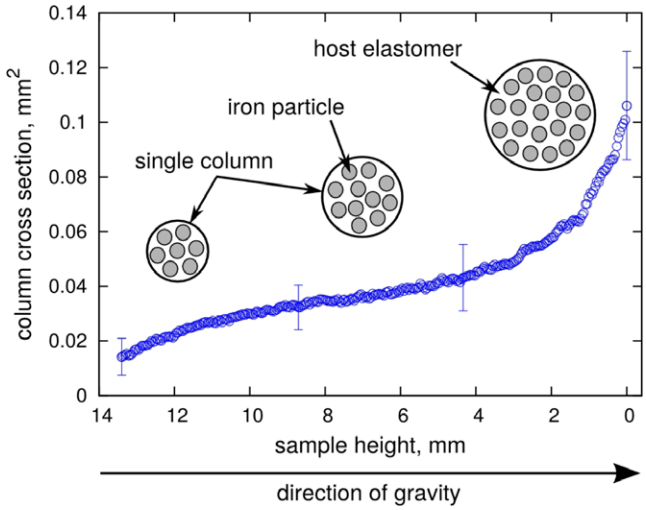


**Figure 10.** Column average cross section versus sample height—patterns of the batch $MRE_1$.

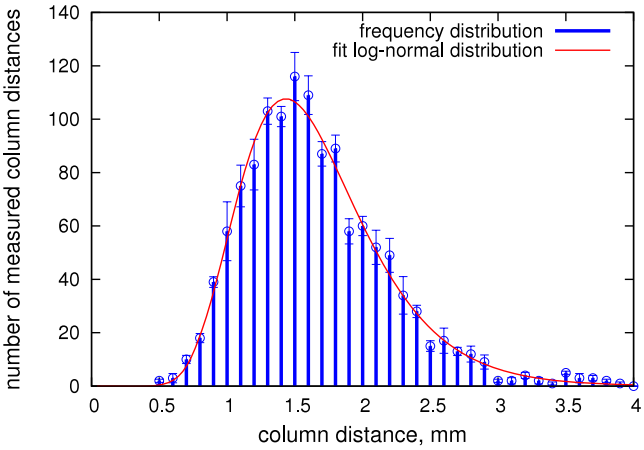


**Figure 11.** Frequency distribution and log-normal fit of the column distances of the samples $MRE_1$.

the top of the rods of $MRE_2$ in figure 6, detailed CT-images were taken with a much higher resolution (figure 9). For this purpose, the CT-parameters were modified. The tube mode has been changed so that the focal spot diameter was now less than 1 $\mu$m. The tube voltage was set to 87 kV with a tube current of 330 $\mu$A and an exposure time of 11 s.

Particle agglomerates are formed. The particles do not form narrow column strands, but thickened branch formations. They are surrounded on all sides with elastomer and are permeated by it.

## 4. Discussion

It has already been noted qualitatively, that the column diameter of the batch $MRE_1$ was larger in the lower part of the samples, than in the top regarding the direction of gravity. Figure 10 shows the profile of the column cross-sectional area depending on the sample height for the three produced samples $MRE_1$. The graph also includes the standard deviation of four slices.

The graph is an average of 16 columns measured per sample. The column cross section increased from an average of 0.01 to 0.11 mm$^2$. Besides the column cross-sectional area, the number of columns was determined. For this, five measurement areas with a diameter of 7.5 mm were defined and placed on the sample cross section. Only columns with a cross-sectional area larger than 0.02 mm$^2$ were registered. The measurement showed that not only the column cross section, but also the number of the columns increased at the bottom of the samples. On average, 0.8 columns mm$^{-2}$ were counted at the sample base. For the assessment of the MRE-structure also knowledge of the average column spacing is crucial. Because the measuring of individual distances turns out to be difficult and too much variation would be the result, a large number of columns were marked with measuring points. These were networked using the Delaunay triangulation [13]. The frequency distribution of column distances of the samples $MRE_1$ is shown in figure 11.

The column distances follow a log-normal distribution. The average spacing is about 1.6 $\pm$ 0.3 mm. The measured

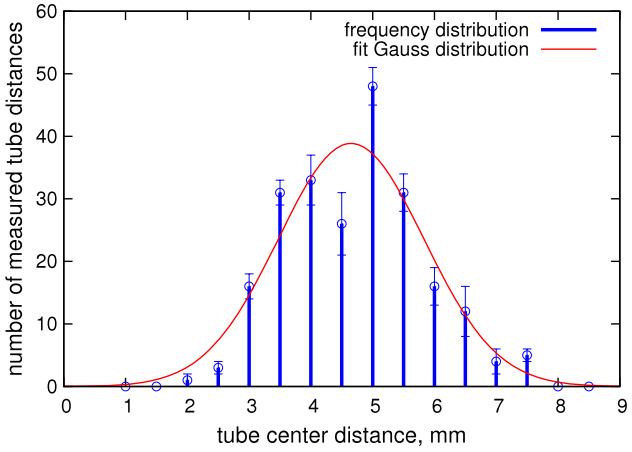


**Figure 12.** Frequency distribution and Gaussian fit of the tube center distances of the samples $MRE_2$.

**Table 2.** Equation and parameters of the log-normal fit function of figure 11.

| Equation | $y_G = \frac{A}{\sqrt{2\pi}wx} \exp[-\frac{(\ln \frac{x}{x_c})^2}{2w^2}]$ | |
|---|---|---|
| Adj. $R$-square | 0.985 | |
| Parameter | Value | Standard deviation |
| Scale parameter, $x_c$ | 1.578 | 0.110 |
| Shape parameter, $w$ | 0.311 | 0.007 |
| Amplitude, $A$ | 126.130 | 2.336 |

column spaces larger than 3.5 mm are due to bad networking at the edges of the measuring area. The parameters of the log-normal fit function are shown in table 2.

Similar to the column spacing of the samples $MRE_1$ the distance of the tube structures of the batch $MRE_2$ was also measured at the sample base. This dimension refers to the center of the tubes. As can be seen in figures 5–8, this distance hardly varies over the specimen height. The distribution of the tube spacing is shown in figure 12. The data have been fitted with a Gaussian function. The equation with the associated parameters is shown in table 3

The tube center spacing is approximately $4.7 \pm 1.2$ mm. The coefficient of determination is lower than for the batch $MRE_1$.

As seen, the statistical dispersion of distance values compared with those of table 2 is larger. This fact is due to the lower number of possible measuring lines, resulting from the reduced number of tubes compared to the number of columns of the samples $MRE_1$. Besides the tube center spacing also the outer tube diameter was determined. On average this was $3.0 \pm 0.60$ mm at the sample base. As already mentioned in section 3, these tubes close with increasing sample height. The cause of the formation of such particle formations could be attributed to a superposition of the gravitational influence and the repulsive forces acting between the particles.

The inner vacancies that occurred both in samples $MRE_3$ and $MRE_4$, suggest that a critical density of the magnetic particles was achieved. The strong magnetic field and the associated high magnetization of the filler results in a strong

**Table 3.** Equation and parameters of the Gaussian fit function of figure 12.

| Equation | $y_G = \frac{A}{w\sqrt{\pi/2}} \exp[-2\frac{(x-x_c)^2}{w^2}]$ | |
|---|---|---|
| Adj. $R$-square | 0.876 | |
| Parameter | Value | Standard deviation |
| Scale parameter, $x_c$ | 4.65 | 0.113 |
| Shape parameter, $w$ | 2.36 | 0.23 |
| Amplitude, $A$ | 114.88 | 9.55 |

interaction between the particles. The resulting magnetic forces cause repulsion of identically aligned regions. However, this alone cannot explain the inhomogeneous appearance of the meanders. In combination with the viscous forces and the volume change that act during curing, a partial cluster breakup is supported and initiated. Likewise, a temperature-related influence is possible.

## 5. Summary

The main objective of the paper was the examination by CT of the anisotropic MRE-structure dependence of the mass fraction of the magnetic filler. The mass fraction was varied in ~10% increments, starting at ~5 wt% iron powder. Even such small variations in the mass concentration were sufficient to achieve a completely different phase constitution.

Besides the column spacing of the samples $MRE_1$, the distances between the centers of the tubes of the samples $MRE_2$ were determined. The latter was about three times larger than the column spacing. The increasing cross-sectional area of the columns of samples $MRE_1$ could be attributed to the influence of gravity, which has a significant impact during the manufacturing process. This results in a density gradient of the samples. The same is true for the samples $MRE_2$. Here, an enlarged tube diameter at the sample base was measured. In addition, a possible explanation for the origin of meanders for samples with a mass content above ~23% of iron powder was given. The preparation of MREs is a complex process which depends on many parameters. Other factors which affect the phase structure may also be the degree of mixing of the polymer in the viscous state with the particles, the polymerization temperature, the temperature gradient and the strength of the applied magnetic field.

## Acknowledgments

This project is funded by the European Union (ERDF) and the Free State of Saxony.

## References

[1] Jolly M R, Carlson J D and Munoz B C 1996 *J. Intell. Mater. Syst. Struct.* **7** 61322
[2] Carlson J D and Jolly M R 2000 *Mechatronics* **10** 555
[3] Zhang W, Gong X, Sun T, Fan Y and Jiang W 2010 *Chin. J. Chem. Phys.* **23** 226–30
[4] Böse H 2007 *Int. J. Mod. Phys.* B **21** 4790–7

[5] Bossis G, Volkova O, Lacis S and Meunier A 2002 *Ferrofluids: Magnetically Controlable Fluids and Their Applications* ed S Odenbach (Berlin: Springer) pp 202–30
[6] Chen L, Gong X L and Li W H 2008 *Polym. Test.* **27** 340–5
[7] Stepanov G V, Abramchuk S S, Grishin D A, Nikitin L V, Kramarenko E Yu and Khokhlov A R 2007 *Polymer* **48** 488–95
[8] Stepanov G V, Borin D Yu, Raikher Yu L, Melenev P V and Perov N S 2008 *J. Phys.: Condens. Matter* **20** 204121
[9] Zhou G Y 2003 *Smart Mater. Struct.* **12** 139–46
[10] Zhang W, Gong X L and Chen L 2010 *J. Magn. Magn. Mater.* **322** 3797–801
[11] Chen L, Gong X L and Li W H 2007 *Smart Mater. Struct.* **16** 2645–50
[12] Balasoiu M, Craus M L, Anitas E M, Bica I, Plestil J and Kuklin A I 2010 *Phys. Solid State* **52** 917–21
[13] Hjelle Ø and Dæhlen M 2006 *Triangulations and Applications* (Berlin: Springer)